Real-time observation of bacteriophage T4 gp41 helicase reveals an unwinding mechanism

Timothée Lionnet*†, Michelle M. Spiering‡, Stephen J. Benkovic‡§, David Bensimon*, and Vincent Croquette*

*Laboratoire de Physique Statistique, Ecole Normale Supérieure, Centre National de la Recherche Scientifique-UMR8550, 24 Rue Lhomond, 75005 Paris, France; and ‡Department of Chemistry, Pennsylvania State University, 104 Chemistry Building, University Park, PA 16802

Contributed by Stephen J. Benkovic, October 17, 2007 (sent for review September 29, 2007)

Helicases are enzymes that couple ATP hydrolysis to the unwinding of double-stranded (ds) nucleic acids. The bacteriophage T4 helicase (gp41) is a hexameric helicase that promotes DNA replication within a highly coordinated protein complex termed the replisome. Despite recent progress, the gp41 unwinding mechanism and regulatory interactions within the replisome remain unclear. Here we use a single tethered DNA hairpin as a real-time reporter of gp41-mediated dsDNA unwinding and single-stranded (ss) DNA translocation with 3-base pair (bp) resolution. Although gp41 translocates on ssDNA as fast as the *in vivo* replication fork (≈400 bp/s), its unwinding rate extrapolated to zero force is much slower (≈30 bp/s). Together, our results have two implications: first, gp41 unwinds DNA through a passive mechanism; second, this weak helicase cannot efficiently unwind the T4 genome alone. Our results suggest that important regulations occur within the replisome to achieve rapid and processive replication.

passive mechanism | single molecule | magnetic tweezers | DNA replication | replisome

Bacteriophage T4 replication machinery, an eight-protein complex termed the replisome, is able to promote phage genome replication at rates of 400 bp/s *in vivo* (1) and constitutes an attractive model for prokaryotic DNA replication. The separation of the parent double helix, a necessary step in the progress of the replication fork, is achieved by the bacteriophage T4 helicase gp41. Helicases are motor proteins involved in nearly every aspect of nucleic acid metabolism (2). However, the mechanism by which they couple ATP hydrolysis to the unwinding of the double helix is not yet fully understood. In particular, it is not clear whether they act by an active mechanism whereby the helicase actively destabilizes the double helix or by a passive mechanism where the enzyme is a mere ssDNA translocase trapping the spontaneous opening fluctuations of the fork (3–5). In this passive scheme, ATP hydrolysis is used only to generate directed motion of the enzyme on its track. Single-molecule experiments have proven to be a powerful tool to study this question (6, 7). In particular, it has been suggested that T7 replicative helicase actively unwinds DNA (8). Two models accounting respectively for RNA and DNA unwinding by HCV NS3 helicase also are consistent with an active mechanism (9, 10). However, it is still unclear whether all helicases unwind nucleic acids employing an active mechanism.

gp41 is a hexameric (11, 12), DnaB-like helicase that unwinds DNA with 5′ to 3′ polarity (13). It forms a stable complex with six units of the gp61 primase when ssDNA or forked DNA is present (14). Helicase activity has been shown to be stimulated upon association with gp61 or in coupled assays with the DNA polymerase gp43 (13, 15–17). However, the underlying mechanism of base-pair unwinding still is unknown. To obtain a full picture of the interactions between gp41 and its partners within the replisome, it is crucial first to characterize gp41 helicase activity in isolation.

Here we use magnetic tweezers (18, 19) to measure the rate of gp41 as it unwinds dsDNA or translocates on ssDNA. By varying the force destabilizing the DNA substrate and the ATP concentration, we probe the gp41 unwinding mechanism.

Results

Experiments were carried out by tethering a DNA hairpin between a glass surface and a magnetic bead [Fig. 1*A*, supporting information (SI) Fig. 6*A*]. Two DNA substrates were used in this study with respective duplex lengths of 231 bp and 6.8 kbp. By positioning two magnets above the sample, we applied a controlled force on the DNA hairpin. The basis of the assay is as follows: gp41-catalyzed unwinding of the hairpin results in an increase in the end-to-end distance of the DNA molecule observed as a change in the distance between the bead and the surface (Fig. 1*A*).

We initially characterized the mechanical unfolding of the hairpin construct in the absence of gp41. Mechanical unfolding resulting in an extension of the DNA molecule occurs at a typical force of 14.1 ± 1 pN and displays a marked hysteresis (SI Fig. 6*B*) (20, 21). At forces $F \leq 11 \pm 1$ pN, the hairpin is stably folded for the duration of a typical experiment. Therefore, below 11 ± 1 pN of force, any unfolding observed in the presence of gp41 results from its activity. Indeed, in the absence of helicase, the extension of the DNA molecule remains constant at the level corresponding to the folded hairpin.

After this calibration, the DNA hairpin was held at a constant force below the unfolding transition, a buffer containing the protein and ATP was injected into the experimental chamber, and the extension of the molecule was recorded over time. Any change in extension thus is attributable to an interaction of the helicase with the DNA (unwinding, dissociation, or translocation on ssDNA).

gp41 Unwinding Rate Measurement. As gp41 and ATP were added, we observed short events displaying a transient increase of DNA extension (Fig. 1*B*). Between these events, the measured length of the DNA molecule corresponds to the folded state of the hairpin. The slope of the DNA extension time trace during these events (i.e., the unwinding velocity) depends on the ATP concentration (see below). Thus, these events result from helicase-catalyzed transient unwinding of the duplex. The time duration of each event is much shorter than the time between events, which guarantees that each event results from the activity of a single helicase complex. The length increase (in nanometers) we observed can be readily translated into base pairs at a given force

Author contributions: T.L. and M.M.S. performed research; T.L. and V.C. analyzed data; and T.L., M.M.S., S.J.B., D.B., and V.C. wrote the paper.

The authors declare no conflict of interest.

†To whom correspondence may be sent at the present address: Department of Anatomy and Structural Biology, Albert Einstein College of Medicine, 1300 Morris Park Avenue, Bronx, NY 10461. E-mail: tlionnet@aecom.yu.edu.

§To whom correspondence may be addressed at: Department of Chemistry, Pennsylvania State University, 414 Wartik Laboratory, University Park, PA 16802. E-mail: sjb1@psu.edu.

This article contains supporting information online at www.pnas.org/cgi/content/full/0709793104/DC1.

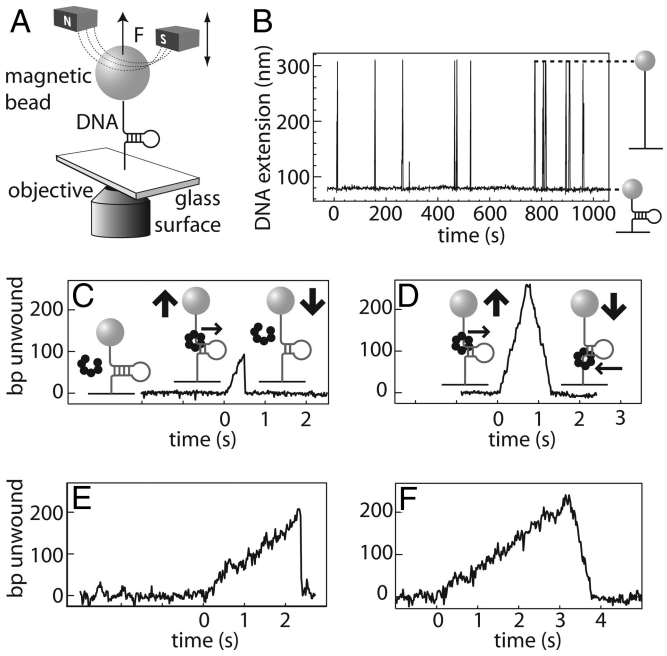

Fig. 1. DNA unwinding by gp41. (*A*) Experimental setup. Two magnets exert a controlled force on a magnetic bead tethered to a single DNA hairpin. (*B*) gp41 activity on the 231-bp hairpin results in a series of well separated, transient DNA extension events. In the conditions used here ([ATP] = 5 mM; F = 10 pN), the vast majority of events result in the full unwinding of the duplex. (*C* and *D*) Two types of events are observed on the 231-bp substrate: the first type (*C*) displays a slowly rising edge caused by DNA unwinding and a fast falling edge corresponding to spontaneous DNA rehybridization upon gp41 dissociation; the second type (*D*) displays a slowly rising edge until the duplex is fully open followed by a slowly falling edge corresponding to rezipping or the fork closing in the protein's wake ([ATP] = 5 mM; F = 10 pN). Thin arrows indicate gp41 motion, and thick arrows indicate bead motion. (*E* and *F*) The two types of events also are observed at lower force ([ATP] = 5 mM; F = 6 pN). (*E*) Unwinding followed by rapid spontaneous reassociation of the two strands. (*F*) Unwinding followed by rezipping. The unwinding rate depends on the force (compare rising edge slopes of *C* and *D* versus *E* and *F*), whereas the rezipping rate is force-independent (compare the falling edge slope of *F* versus that of *D*).

by using the measured ssDNA extension versus force curve (22, 23). This conversion factor is calibrated against the full length of the hairpin, measured as the maximal length of the unwinding events (*SI Text* and SI Fig. 7).

Two types of events were observed. The first type consists of a slowly rising edge followed by a rapidly falling edge (Fig. 1 *C* and *E*). The length of these events is variable, distributed between zero and full DNA extension. In contrast with the ATP-dependent slope of the rising edge, the falling edge displays a steep, ATP-independent slope, which means that although the rising edge is gp41-controlled, the falling edge is not. As a consequence, the rising edge must correspond to gp41 unwinding the duplex, whereas the falling edge must correspond to the spontaneous reannealing of the two strands. It is highly unlikely that the two strands rehybridize around the helicase (*SI Text*). We therefore conclude that the first type of event corresponds to gp41 unwinding the duplex, then dissociating from its DNA substrate, allowing the two DNA strands to reanneal, refolding the hairpin completely.

The second type of event displays a slowly rising edge until the maximum DNA extension is reached (i.e., fully unwound hairpin) followed by a slowly falling edge (Fig. 1 *D* and *F*). These events all display full-length unwinding of the duplex. Both the rising and falling rates are dependent on the ATP concentration (although they are not necessary equal; see Fig. 1*F*). The slowly rising edge displays the same slope as the rising edge in the first type of event. We therefore conclude that it corresponds to gp41 unwinding the entire duplex. The falling edge also must correspond to gp41 activity because it is ATP-dependent as well. It is highly unlikely that the falling edge is caused by the presence of a second helicase because the probability of coincident binding of two helicases at low concentration is negligible, or that the helicase switches directionality at the center of the hairpin [previous experiments have shown that gp41 translocates with a 5′ to 3′ polarity (13)]. It also is unlikely that gp41 could switch strands as reported for other helicases (8, 24), because we would expect such events to occur randomly during unwinding and not only in situations with a fully unfolded hairpin. We therefore conclude that this type of event corresponds to the helicase unwinding the entire duplex and then translocating further on the ssDNA, thus blocking the spontaneous, rapid rehybridization of the two separated strands. As the helicase moves on the ssDNA, the fork is able to slowly close in its wake. Thus, the falling edge corresponds to the gp41 translocation-limited rezipping of the opened hairpin.

The unwinding rate v_U can be measured from the slope of the rising edge. We define the rezipping rate v_Z as the slope of the slowly falling edge (*SI Text* and SI Figs. 8–10). The rezipping velocity is ATP concentration-dependent (typically a few hundred base pairs per second) and can be readily distinguished from the fast, ATP concentration-independent spontaneous rehybridization rate (typically a few thousand base pairs per second). Although the unwinding rate increases with increasing force, the rezipping rate does not depend on the applied force (compare Fig. 1 *C* versus *E* and *D* versus *F*).

gp41 Rezipping Rate Is Equal to Its ssDNA Translocation Rate. During the rezipping phase, the enzyme translocates on ssDNA, and the fork closes in its wake. Is this situation different from gp41 translocating alone on ssDNA? The fork closing behind the enzyme might alter the enzyme translocation rate in two possible, but not mutually exclusive, ways: first, the pairing energy gained by the fork while it is closing might provide an effective driving force to the translocating helicase, and second, the mere presence of the fork in the vicinity of gp41 might affect its velocity.

We addressed the first point by measuring the gp41 rezipping rate v_Z as a function of force. At low force ($F \approx 3$ pN), the folded hairpin is highly stable; therefore, the potential driving force exerted by the fork should be the greatest. In contrast, when approaching the mechanical unfolding transition ($F \approx 12$ pN), the effective driving force should approach zero because the paired and unpaired forms of the hairpin are equally stable at the transition. Therefore, one would expect significant changes in the driving force between 3 and 12 pN that should reflect on v_Z. We find that the rezipping rate v_Z does not depend on the force exerted (compare Fig. 1 *D* and *F*; Fig. 2*A*). Therefore, we conclude that the pushing action of the closing fork caused by the energy gain upon base-pairing is negligible.

To address the influence of the presence of the fork behind gp41, we performed the following experiment. We increased the force to a value close to the unfolding transition. In this regime, the folded hairpin is stable on the time scale of the experiment; however, if previously unfolded, the spontaneous rehybridization of the two strands does not take place immediately but after a fraction of second. We then recorded gp41 unwinding events. In addition to the two main types of events described above, we observed a third type (Fig. 2*B*). After a careful evaluation of the other potential interpretations for these events (*SI Text*), we dismiss them and conclude that these events correspond to a single enzyme unwinding dsDNA (Fig. 2*Ci*) and continuing to translocate on ssDNA, first without any fork behind it (Fig. 2 *Cii*

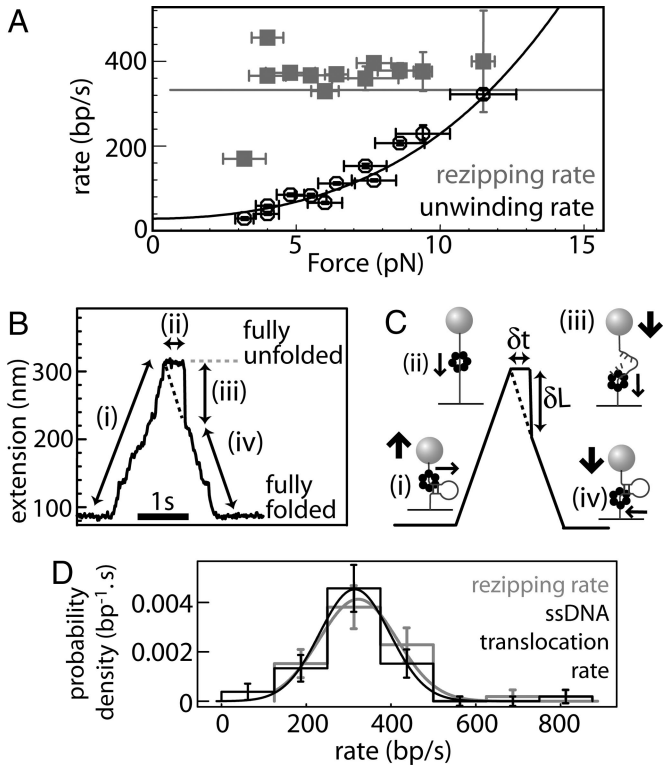

Fig. 2. Unwinding rate v_U and rezipping rate v_Z measured as a function of force at saturating ATP concentration. (*A*) The unwinding rate (black circles) displays a 10-fold increase as the force is increased from 3 to 11.5 pN. The rezipping rate (gray squares) does not display any significant variation over the force range explored ([ATP] = 5 mM, [gp41] = 100 nM monomer, 6.8-kbp substrate). (*B*) Events observed on the 231-bp substrate in the high force regime displaying four phases: (*i*) complete duplex unwinding by gp41; (*ii*) short extension plateau at the fully unfolded state; (*iii*) rapid, spontaneous rehybridization of the two DNA strands up to the helicase position; and (*iv*) gp41 rezipping with the fork closing in its wake. This type of event allows for the direct comparison of the rezipping rate (slope of phase *iv*) with the ssDNA translocation rate by gp41 on the stretched ssDNA (slope of the black dotted line; see text). $F = 9 \pm 1$ pN, [ATP] = 5 mM, [gp41] = 100 nM monomer, 231-bp substrate. (*C*) Schematic representation of the event displayed in *B*. The ssDNA translocation rate is equal to $\delta L/\delta t$, or equivalent to the slope of the dashed line. (*D*) Rezipping rate distribution and ssDNA translocation rate distribution measured on events displayed in *B*. The histograms were fit to Gaussian distributions, yielding averages of 322 ± 17 bp/s (SD 92 bp/s) for the rezipping rate (gray) and 314 ± 15 bp/s (SD 83 bp/s) for the ssDNA translocation rate (black); $F = 9 \pm 1$ pN, [ATP] = 5 mM, [gp41] = 100 nM monomer, 231-bp substrate; $N = 43$ events.

and C*iii*), then with the fork closing in its wake (Fig. 2C*iv*). We can measure the rezipping rate during these events as the slope of the extension time trace during phase (Fig. 2C*iv*). In contrast, the translocation of the enzyme on the stretched ssDNA does not change its extension; however, we can estimate this rate as the ratio of the distance traveled divided by the time the hairpin remains unfolded ($\delta L/\delta t$ in Fig. 2*C*). We then compare the rates of translocation on ssDNA with or without a fork closing behind the helicase. In the conditions explored ($F > 7$ pN; 0.5 mM $\leq$ [ATP] $\leq$ 5 mM), the mean rates are similar (Fig. 2*D*), differing by only 5% (SD 20%; $N = 10$ events).

We therefore conclude that the rezipping rate is equal to the ssDNA translocation rate. As a consequence, we can measure the dsDNA unwinding rate and the ssDNA translocation rate under the exact same conditions to quantify how gp41 slows down while unwinding dsDNA as compared with when it translocates on ssDNA. These measurements, performed as a function of force and ATP concentration, provide us with a set of data amenable to test various helicase mechanisms.

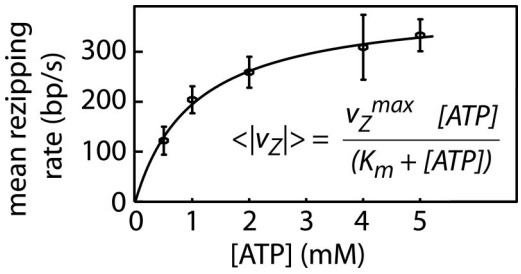

Fig. 3. Force-averaged rezipping velocity. $\langle |v_Z| \rangle$ (ssDNA translocation velocity; see text) as a function of ATP concentration. The rezipping velocity obeys Michaelis–Menten kinetics with a maximum rate $v_Z^{max} = 400 \pm 10$ bp/s and $K_m = 1.1 \pm 0.1$ mM; data collected on the 6.8-kbp substrate (*SI Text*).

ssDNA Translocation Does Not Involve Cooperative ATP Hydrolysis. We first characterized the ssDNA translocation rate dependency on ATP. For each ATP concentration, we obtained the ssDNA translocation rate as the average of the force-independent rezipping rates (Fig. 3). The resulting ssDNA translocation velocity versus ATP concentration curve was fit to the Michaelis–Menten equation, $\langle |v_Z| \rangle = v_Z^{max}$ [ATP]/(K_m + [ATP]), with a maximum velocity (v_Z^{max}) of 400 ± 10 bp/s and K_m of 1.1 ± 0.1 mM. The observed nonsigmoidal kinetics rule out a translocation mechanism involving simultaneous ATP hydrolysis by the six helicase monomers but cannot distinguish between independent or cooperative ATP binding. Based on this result, we have modeled gp41 translocation on ssDNA involving a reversible ATP binding step followed by an irreversible translocation event (Fig. 4*A*).

Global Model for Helicase Activity. Next, we measured the dsDNA unwinding rate v_U as a function of applied force and ATP concentration (Fig. 5*A*). The unwinding rate increases continuously with increasing force and ATP concentration. The maximum unwinding velocity measured at the critical force where the hairpin is marginally stable ($F \approx 12$ pN) agrees with the translocation velocity on ssDNA (Fig. 2*A*) at the same ATP concentration.

We represent these results by using a simple global model for helicase activity on ssDNA and dsDNA (Fig. 4). We assume that the enzyme first binds ATP reversibly and that translocation is coupled to ATP hydrolysis. In the case of ssDNA translocation, the enzyme step size is n bp and occurs with rate k_+ (Fig. 4*A*). In the case of dsDNA unwinding (Fig. 4*B*), the fork must open by n bp before translocation. The kinetics of fork opening/closing depend on the force exerted to open the hairpin and the active/passive character of the helicase. Finally, translocation by n bases takes place with the same rate k_+ as on ssDNA.

The active/passive nature of the helicase is introduced in to the model through the fork opening and closing rates, α and β, respectively, following a recent model (3, 25). Briefly, if the enzyme is passive, the opening/closing kinetics of the fork are unaffected by the presence of the helicase. In contrast, as defined here, an active helicase directly destabilizes the double helix. As a result, α and β depend on the position of the enzyme relative to the fork. When the enzyme is at the fork, the opening step is favored over the closing one. This active mechanism is modeled by lowering the energy of unpairing at the fork (i.e., the equilibrium constant α/β) by a fixed amount when the enzyme is within n bp of the fork. The amount of energy contributed by the enzyme to the destabilization of the junction constitutes a measure of the active character of the enzyme. We assume that the base-pairing energy is homogenous, thus neglecting sequence effects. To preserve generality, we present here a simple version of the model assuming that destabilization by the helicase occurs on the range of its step size and neglecting activation barrier position effects (25).

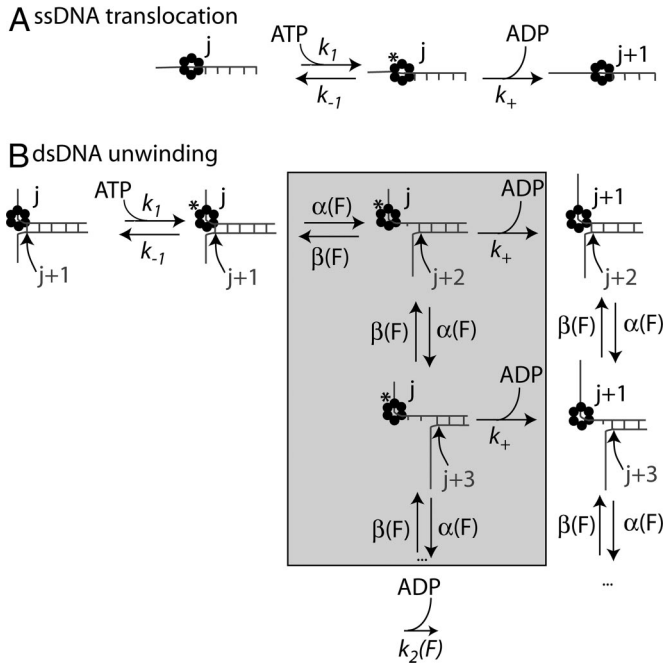

Fig. 4. Proposed kinetic scheme. For clarity, the enzyme is drawn performing 1-bp steps; however, the step size is a free parameter of the model. (*A*) Model for ssDNA translocation includes reversible ATP binding followed by ATP hydrolysis and translocation by one step. The star denotes the ATP-bound enzyme. (*B*) Model for dsDNA unwinding. ATP binding and translocation steps have the same rate constants as in the ssDNA case (*A*). The enzyme can only perform the translocation step if the next *n* bp (the enzyme step size) is open. DNA opening and closing is modeled by the force-dependent rate constants α and β. If the enzyme is passive, these rates do not depend on the position of the enzyme relative to the fork. However, in the case of an active helicase, the presence of the enzyme at the fork destabilizes the junction; therefore, α and β depend both on the force exerted and on the relative distance of the helicase to the fork. Steps within the gray box (the force-dependent and translocation steps) can be combined in a unique step represented as $k_2(F)$, where k_2 depends on the force, the step size of the helicase, and the type of unwinding mechanism (active versus passive).

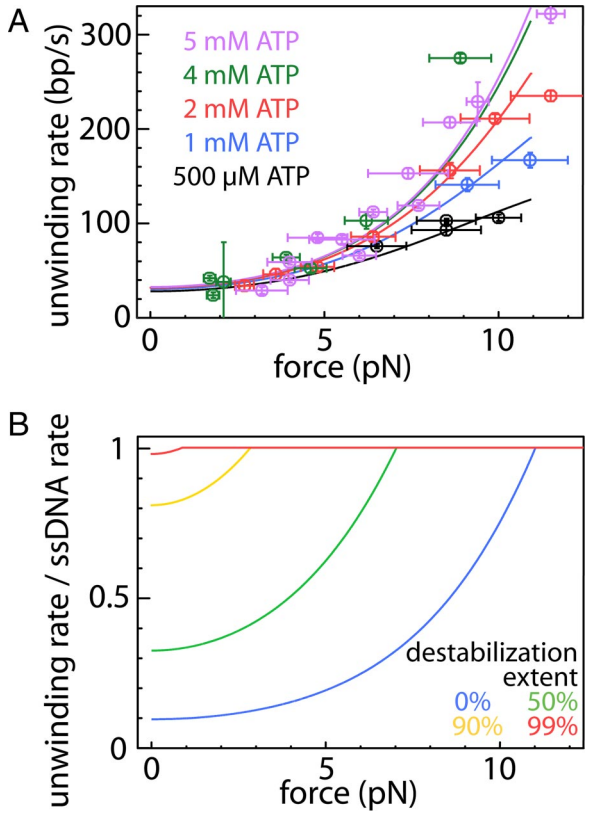

Fig. 5. Dependence of the unwinding rate v_U on the force *F*. (*A*) Unwinding rate versus force at various ATP concentrations. Circles, experimental data ($N = 100$ events typically, 6.8-kbp substrate; *SI Text*); solid lines, fit to the helicase kinetic model (see text). Global fitting of the data yields the number of base pairs opened in one enzymatic cycle as $n = 1.4 \pm 0.25$ bp and the effective base-pairing energy at zero force as $\Delta G_0 - \Delta G_{\text{Heli}} = 1.9 \pm 0.25\ k_BT$. (*B*) Unwinding rate normalized to the ssDNA translocation rate versus force curves calculated for theoretical helicases varying in their level of double helix destabilization. Blue, 0% destabilization (a perfectly passive helicase); green, 50% destabilization; yellow, 90% destabilization; red, 99% destabilization. Extent of destabilization is given as the ratio of the energy input by the helicase divided by the average base-pairing energy in the absence of force: $\Delta G_{\text{Heli}}/\Delta G_0$, (where $\Delta G_0 = 1.95\ k_BT$). Except for ΔG_{Heli}, the rates and step size are equal to those found for gp41 in our experiments; [ATP] = 5 mM. As the energy input increases, the unwinding rate reaches the ssDNA translocation rate (high force plateau observed for all curves) more rapidly. At $F = 0$, the unwinding rate of an optimally active helicase would be very close to the ssDNA translocation rate.

By using this model, the effective translocation rate k_2 corresponding to DNA opening followed by translocation (Fig. 4*B*) can be calculated (3, 25):

$$k_2(F) = nk_+(\alpha/\beta)^n = v_Z^{\max}(\alpha/\beta)^n. \quad [1]$$

Thus, the unwinding rate is equal to the maximum helicase ssDNA translocation rate $v_Z^{\max}$ times the probability that the next *n* bp are opened. This property holds provided that (*i*) the fluctuations of the fork are fast compared with the translocation rate k_+ (fraying time scales have been estimated in the microsecond range (25–28) compared with the measured ssDNA translocation rate of millisecond per base pair), and (*ii*) the helicase very rarely steps backwards (we did not observe experimentally any evidence suggesting backwards stepping).

We rewrite k_2 using the effective free energy cost $\Delta G_{\text{bp}}(F)$ to open 1 bp:

$$k_2(F) = v_Z^{\max}\exp\left(-n\,\frac{\Delta G_{\text{bp}}(F)}{k_BT}\right). \quad [2]$$

The effective base-pairing energy $\Delta G_{\text{bp}}(F)$ consists of a positive, force-independent contribution ΔG_0 (the binding energy) and two negative ones: ΔG_{Heli}, induced by helicase destabilization (equal to zero if the helicase is passive) and ΔG_F, which results from the force destabilizing the junction:

$$\Delta G_{\text{bp}}(F) = \Delta G_0 - \Delta G_{\text{Heli}} - \Delta G_F. \quad [3]$$

The force-dependent contribution ΔG_F comprises both the enthalpy associated with the work done by the force to separate the strands and the entropy of the ssDNA segments (*SI Text*) and can be explicitly calculated. Therefore, k_2 becomes

$$k_2(F) = v_Z^{\max}\exp\left(-n\,\frac{\Delta G_0 - \Delta G_{\text{Heli}}}{k_BT}\right)\exp\left(n\,\frac{\Delta G_F}{k_BT}\right). \quad [4]$$

According to Eq. **4**, the unwinding rate at saturating ATP will depend on the force *F* for both active and passive helicases. However, a passive helicase ($\Delta G_{\text{Heli}} = 0$) will display a steeper increase in k_2 with increasing force than an active helicase ($\Delta G_{\text{Heli}} > 0$). Finally, we compute the global rate of unwinding as

$$v_U = \frac{k_2(F)[\text{ATP}]}{[\text{ATP}] + (k_2(F) + k_{-1})/k_1} \approx \frac{k_2(F)[\text{ATP}]}{[\text{ATP}] + k_2(F)/k_1}. \quad [5]$$

BIOCHEMISTRY

Using Eq. **5**, we globally fit the measured unwinding rates $v_U(F, [\mathrm{ATP}])$. The free parameters are the step size n and the effective base-pairing energy at zero force $\Delta G_0 - \Delta G_{\mathrm{Heli}}$ (Fig. 5*A*). We impose that above the force where $\Delta G_{\mathrm{bp}}(F) = 0$, where ssDNA and dsDNA are equally stable, the dsDNA rate equals the ssDNA translocation rate. The best fit is obtained when $n = 1.4 \pm 0.25$ bp and $\Delta G_0 - \Delta G_{\mathrm{Heli}} = 1.9 \pm 0.25\ k_{\mathrm{B}}T$ (uncertainty includes error in ssDNA elasticity; *SI Text*). For the closest integer values of the step size $n = 1$ or 2 bp, similar values are obtained for $\Delta G_0 - \Delta G_{\mathrm{Heli}}$, 2.3 or 1.6 $k_{\mathrm{B}}T$, respectively. It is possible to estimate ΔG_0 knowing the GC content of the sequence studied. Using values of 1.3 $k_{\mathrm{B}}T$ and 2.9 $k_{\mathrm{B}}T$ for AT and GC base pairs, respectively (29), we obtain $\Delta G_0 = 1.95\ k_{\mathrm{B}}T$ for our 42% GC-rich large DNA molecule, and therefore $\Delta G_{\mathrm{Heli}} = 0.05\ k_{\mathrm{B}}T$ ($-0.2 < \Delta G_{\mathrm{Heli}} < 0.3\ k_{\mathrm{B}}T$). In other words, our results indicate that the destabilization of the double helix by gp41 is very small (<15% of the base-pairing energy), which is consistent with gp41 unwinding DNA by an essentially passive mechanism.

gp41 Processivity. The number of base pairs unwound by gp41 before dissociation (N_U) provides a measure of the enzyme's processivity. The cumulative dissociation distribution $P(N_U < N_{\mathrm{bp}})$, the probability that the enzyme dissociates from its substrate before reaching N_{bp} base pairs, is a convenient way to assess the processivity of gp41 (SI Figs. 11 and 12). The cumulative dissociation distributions have been measured on the 231-bp substrate and fit to an ad hoc function under various forces and ATP concentrations (data not shown). For the various conditions investigated, the processivity of gp41 lies within 100–800 bp, which is considerably smaller than the processivity reported for the entire T4 replisome (15, 30). The large range is attributable to the limited statistics and does not permit us to address the possible dependence of gp41 processivity on ATP concentration or force.

Discussion

Comparisons with Previous Results. The ssDNA velocity measured in these experiments is in agreement with a previous estimate based on bulk ATP hydrolysis measurements of gp41 in the presence of linear or circular ssDNA (17, 31). In previous ensemble measurements, gp41 ATPase activity also displayed a high (millimolar) K_m but with a sigmoidal dependence on the ATP concentration (13, 17). Here we measure the ATP dependence of the translocation step, whereas steady-state ensemble experiments measure the slowest step that limits the rate of turnover. Generally, this is a slow process such as binding or dissociation that might display a different ATP dependence.

The gp41 unwinding rate has been measured in bulk *in vitro* assays where the helicase was loaded on the DNA molecule with the loader protein gp59 (32). An unwinding rate of 30 bp/s was reported, in excellent agreement with our data extrapolated to zero force.

gp41 Step Size. The comparison of our data to a simple model suggests a 1.4-bp step size for gp41. Similar experiments on the related T7 helicase (8) reported a 2-bp step size. In contrast, a 1-bp step size value has been reported for *E. coli* replicative helicase DnaB (33), the archetypal member of the DnaB-like helicase superfamily. These results relate to the kinetic step size of the enzyme, defined as the average number of base pairs unwound between two rate-limiting steps. The kinetic step size might actually consist of sequential rapid substeps whose size (the structural step size) corresponds to the minimal discrete motion of the enzyme. A 1-bp structural step size seems more likely, in light of structural results obtained for the papillomavirus hexameric replicative helicase E1 (34). Such a small step size reveals a highly inefficient helicase: one ATP hydrolysis event releases 12 kcal/mol or ≈20 $k_{\mathrm{B}}T$ (at room temperature) worth of energy, ≈10 times more than the base-pairing energy.

gp41 Mechanism Implications. The comparison of our results with a very simple model suggests that gp41 unwinds DNA by using a passive mechanism. This picture is consistent with an exclusion model of DNA unwinding in which the hexameric ring translocates on ssDNA while excluding the other strand from its central channel (35). The pairing energy of the strands acts as a force opposing the DNA opening accounting for the slower unwinding rate of gp41 compared with its ssDNA translocation rate. Note that our description neglects sequence heterogeneity effects, potential deformations of the DNA strands, and complex possible interactions of each separated strand with the helicase. We therefore do not exclude that a more elaborated model might yield a different result.

Our findings do not rule out that other classes of helicases may use active mechanisms. Indeed, superfamily 1 (SF1) helicase PcrA (36) has been reported to unwind DNA by using an active mechanism. Also, SF1 UvrD helicase features a dsDNA unwinding rate much closer to its ssDNA translocation rate [$v_{\mathrm{ssDNA}}/v_{\mathrm{dsDNA}} \approx 1.2$ or 2.8 for UvrD (24, 37)], which might reflect a more active mechanism for UvrD than gp41 (Fig. 5*B*). In similar experiments on an RNA hairpin under tension, SF2 NS3 helicase displayed no variation of its unwinding rate with the force, suggesting an active mechanism (9, 38). Another group recently proposed a spring-loaded mechanism to account for DNA unwinding by NS3 based on single-molecule FRET experiments (10). In this model, ATP hydrolysis events induce forward motion of two domains of the enzyme. DNA unwinding is accomplished by the mechanical strain built up during such successive cycles. This picture also is consistent with an active mechanism.

Structurally similar to gp41, the T7 replicative helicase gp4 exhibits similar qualitative dynamics in a recent study (8), consistent with previous bulk experiments (39). There are, however, significant quantitative differences between T7 gp4 and T4 gp41: (*i*) T7 gp4 is reported to switch strands, a feature we never observed with gp41; (*ii*) its processivity is much larger than gp41 (thousands versus hundreds of base pairs); and (*iii*) it appears to destabilize a DNA fork more than gp41 ($\Delta G_{\mathrm{Heli}} \approx 1.2\ k_{\mathrm{B}}T$ versus 0.05 $k_{\mathrm{B}}T$). Based on ΔG_{Heli} values, gp41 is closer to the ideal passive helicase, whereas gp4 stands somewhere between the purely passive unwinding model and the purely active unwinding model. However, it must be pointed out that the estimation of ΔG_{Heli} from single-molecule experiments relies on an estimate of the entropic elasticity of the ssDNA unwound by the enzyme, which in the unknown environment of the enzyme might easily be off by 1 $k_{\mathrm{B}}T$ (*SI Text*).

Finally, one must be aware of the pitfalls inherent to the passive/active paradigm. Slightly different definitions of an active mechanism exist depending on whether the base pair destabilization is directly attributable to ATP binding and hydrolysis or only attributable to the presence of the helicase (5, 40). Even so, these definitions do not allow for easy predictive and quantitative experiments to be formulated. Finally, the active/passive classification distinguishes between two extreme cases that do not reflect the continuum of behaviors probably existing in nature.

gp41 Requires Other Proteins to Reach Its Full Speed and Processivity. The gp41 unwinding processivity measured here is similar to the values estimated for gp41 translocation on ssDNA (17, 31) and is notably smaller than those measured in strand displacement synthesis assays catalyzed by gp41 in association with the gp43 DNA polymerase (15, 30).

What are the implications of our results for gp41 activity *in vivo*? The force exerted on DNA *in vivo* may not be strictly zero

because of thermal fluctuations, supercoiling effects, or other cellular processes; however, the small resulting force can be neglected here. Our data suggest that in the absence of an assisting force, the enzyme proceeds at a typical rate of ≈30 bp/s, in agreement with previous results (32). This value is notably slower than the measured *in vivo* replication rate of ≈400 bp/s (41).

Our observations are consistent with previous reports showing that gp41 activity is greatly enhanced by the presence of its replisome partners (16). It is probably beneficial that gp41, when isolated from the replisome, is so slow to avoid extensive unwinding of the DNA. Our data demonstrate that the physiological replication rate is strikingly similar to the maximum unwinding rate of gp41 at high force and the ssDNA translocation rate. Therefore, a specific interaction between gp41 and the other components of the replisome must help the helicase reach its maximum unwinding rate, as reported for the related T7 helicase gp4 (42). The mechanism underlying the gp41 unwinding rate and processivity stimulation is still unclear but might involve destabilization of the DNA junction induced by the presence of the replication complex, specific physical interactions between gp41 and other replisome proteins, and/or the coupling of the unwinding and polymerase activity.

Methods

Protein Purification. The gp41 protein was purified by using the IMPACT system with chitin-based affinity chromatography and a self-cleaving intein followed by anion exchange (Q Sepharose) chromatography as described in ref. 43.

DNA Substrate Preparation. The 6.8-kbp-long DNA hairpin substrate (42% GC) and the 231-bp DNA hairpin (32% GC) were prepared as detailed in *SI Text*.

Single-Molecule Assay. Bead images were acquired at 60 Hz by using a custom-built inverted microscope. Real-time tracking of the bead image yields the DNA extension measurement (18). Force was determined as detailed in *SI Text*. All experiments were performed at 25°C in 25 mM Tris-Ac, pH 7.5, 150 mM KOAc, 10 mM $MgOAc_2$, 1 mM DTT, and the indicated concentration of ATP. We used gp41 monomer concentrations in the 80–500 nM range (*SI Text*).

Data Analysis. Statistics on the unwinding and rezipping rates were collected from time traces recorded on the 6.8-kbp DNA substrate (*SI Text*). Statistics on the processivity of gp41 were extracted from time traces recorded on the 231-bp DNA substrate (*SI Text*).

We thank D. R. Leach for help in DNA preparation, M. D. Betterton for helpful discussions, and T. M. Lohman and M. Manosas for critical reading of the manuscript. This work was supported by Association pour la Recherche contre le Cancer (ARC), Centre National de la Recherche Scientifique, University Pierre and Marie Curie–Paris 6, a grant from the Human Frontier Science Program (to V.C. and S.J.B.), a European Union grant Bionano-switch, National Institutes of Health Grant GM013306 (to S.J.B.), and National Institutes of Health Postdoctoral Fellowship GM071130 (to M.M.S.).

1. Benkovic SJ, Valentine AM, Salinas F (2001) *Annu Rev Biochem* 70:181–208.
2. Singleton MR, Dillingham MS, Wigley DB (2007) *Annu Rev Biochem* 76:23–50.
3. Betterton MD, Julicher F (2003) *Phys Rev Lett* 91:258103.
4. Lohman TM, Bjornson KP (1996) *Annu Rev Biochem* 65:169–214.
5. von Hippel PH, Delagoutte E (2001) *Cell* 104:177–190.
6. Lionnet T, Dawid A, Bigot S, Barre FX, Saleh OA, Heslot F, Allemand JF, Bensimon D, Croquette V (2006) *Nucleic Acids Res* 34:4232–4244.
7. Rasnik I, Myong S, Ha T (2006) *Nucleic Acids Res* 34:4225–4231.
8. Johnson DS, Bai L, Smith BY, Patel SS, Wang MD (2007) *Cell* 129:1299–1309.
9. Cheng W, Dumont S, Tinoco I, Jr, Bustamante C (2007) *Proc Natl Acad Sci USA* 104:13954–13959.
10. Myong S, Bruno MM, Pyle AM, Ha T (2007) *Science* 317:513–516.
11. Dong F, Gogol EP, von Hippel PH (1995) *J Biol Chem* 270:7462–7473.
12. Patel SS, Picha KM (2000) *Annu Rev Biochem* 69:651–697.
13. Venkatesan M, Silver LL, Nossal NG (1982) *J Biol Chem* 257:12426–12434.
14. Zhang Z, Spiering MM, Trakselis MA, Ishmael FT, Xi J, Benkovic SJ, Hammes GG (2005) *Proc Natl Acad Sci USA* 102:3254–3259.
15. Schrock RD, Alberts B (1996) *J Biol Chem* 271:16678–16682.
16. Richardson RW, Nossal NG (1989) *J Biol Chem* 264:4725–4731.
17. Young MC, Schultz DE, Ring D, von Hippel PH (1994) *J Mol Biol* 235:1447–1458.
18. Gosse C, Croquette V (2002) *Biophys J* 82:3314–3329.
19. Strick TR, Allemand JF, Bensimon D, Bensimon A, Croquette V (1996) *Science* 271:1835–1837.
20. EssevazRoulet B, Bockelmann U, Heslot F (1997) *Proc Natl Acad Sci USA* 94:11935–11940.
21. Danilowicz C, Coljee VW, Bouzigues C, Lubensky DK, Nelson DR, Prentiss M (2003) *Proc Natl Acad Sci USA* 100:1694–1699.
22. Smith SB, Cui Y, Bustamante C (1996) *Science* 271:795–799.
23. Dessinges MN, Maier B, Zhang Y, Peliti M, Bensimon D, Croquette V (2002) *Phys Rev Lett* 89:248102.
24. Dessinges MN, Lionnet T, Xi XG, Bensimon D, Croquette V (2004) *Proc Natl Acad Sci USA* 101:6439–6444.
25. Betterton MD, Julicher F (2005) *Phys Rev E Stat Nonlin Soft Matter Phys* 71:011904.
26. Frank-Kamenetskii MD (1997) *Phys Rep* 288:13–60.
27. Chen YZ, Zhuang W, Prohofsky EW (1992) *J Biomol Struct Dyn* 10:415–427.
28. Bonnet G, Krichevsky O, Libchaber A (1998) *Proc Natl Acad Sci USA* 95:8602–8606.
29. Bockelmann U, EssevazRoulet B, Heslot F (1997) *Phys Rev Lett* 79:4489–4492.
30. Dong F, Weitzel SE, von Hippel PH (1996) *Proc Natl Acad Sci USA* 93:14456–14461.
31. Liu CC, Alberts BM (1981) *J Biol Chem* 256:2813–2820.
32. Raney KD, Carver TE, Benkovic SJ (1996) *J Biol Chem* 271:14074–14081.
33. Galletto R, Jezewska MJ, Bujalowski W (2004) *J Mol Biol* 343:83–99.
34. Enemark EJ, Joshua-Tor L (2006) *Nature* 442:270–275.
35. Patel SS, Donmez I (2006) *J Biol Chem* 281:18265–18268.
36. Soultanas P, Dillingham MS, Wiley P, Webb MR, Wigley DB (2000) *Embo J* 19:3799–3810.
37. Fischer CJ, Maluf NK, Lohman TM (2004) *J Mol Biol* 344:1287–1309.
38. Dumont S, Cheng W, Serebrov V, Beran RK, Tinoco I, Jr, Pyle AM, Bustamante C (2006) *Nature* 439:105–108.
39. Jeong YJ, Levin MK, Patel SS (2004) *Proc Natl Acad Sci USA* 101:7264–7269.
40. Singleton MR, Wigley DB (2002) *J Bacteriol* 184:1819–1826.
41. Werner R (1968) *J Mol Biol* 33:679–692.
42. Stano NM, Jeong YJ, Donmez I, Tummalapalli P, Levin MK, Patel SS (2005) *Nature* 435:370–373.
43. Valentine AM, Ishmael FT, Shier VK, Benkovic SJ (2001) *Biochemistry* 40:15074–15085.